Polymer Bulletin 57, 785–796 (2006)
DOI 10.1007/s00289-006-0631-2

Polymer Bulletin

Iridescent Colors from Films Made of Polymeric Core-Shell Particles

Xu He, Yi Thomann, Reinhold J. Leyrer (✉), Jens Rieger

BASF Aktiengesellschaft, Polymer Research, 67056 Ludwigshafen, Germany
E-mail: reinhold.j.leyrer@basf.com

Received: 20 June 2006 / Revised version: 21 June 2006 / Accepted: 27 June 2006
Published online: 27 July 2006 –

Summary

Brilliant and angle-dependent iridescent colors were obtained from polymer films produced via colloidal crystallization of monodisperse core-shell particles by drying aqueous dispersions. By variation of the particle size, the brilliant color could be varied throughout the visible spectrum. The color effects of the smooth thin films exhibit excellent thermal and water stability. The morphology of the core-shell particles and the properties of the corresponding films were characterized by dynamic light scattering (DLS), atomic force microscopy (AFM), differential scanning calorimetry (DSC), and reflection spectrum measurements. The results indicate that the brilliance of the film is strongly dependent on size and quality of the crystalline domains.

Introduction

Monodisperse colloidal spheres with diameters in the range of 100nm can be arranged in such a way that mesoscopic and macroscopic crystals are formed [1]. Starting from colloidal dispersions in water the crystal structures are achieved, e.g., by carefully evaporating the water [2], by sedimentation [3], and by exploiting capillary [4,5] or electric field phenomena [6]. Apart from color effects that are the subject of this paper it is interesting to study colloidal crystallization as model for crystallization in general - with the main advantage that the time-scale of colloidal crystallization is by orders of magnitude slower than that in molecular systems [7]. It thus allows for studying the generic phenomena of crystallization in detail with high resolution in time and space. With regard to practical applications colloidal crystals are interesting because of their optical properties. On the one hand, photonic band gap (PBG) material made from colloidal crystals has attracted much attention over the past decade because of its ability to confine and control light [8-11]. For such systems, a large refractive index difference between the units making up the crystal and the interstitials and particular crystal symmetries must be realized [12]. Unfortunately, the general exploitation of PBG crystals as devices has been hindered by the difficulties in creating the periodic dielectric structures possessing complete band gaps at various frequencies, especially in the optical and near-infrared region [5,6]. One practical approach to manipulate the full PBG crystals is inverse duplication of the traditional colloidal crystals that are made from either silica or polymer colloids [13-15]. By this method, inverse colloidal crystal replicas with high refractive index materials are obtained with the potential to

possess the typical PBG features [13,14,17-20]. On the other hand, colloidal crystals without complete PBG properties also have many interesting applications as, e.g., optical filters, nonlinear optical switches and limiters, chemical and mechanical sensors, and high-density data storage devices [21-25].

But also colloidal crystals with relatively small refractive index differences show interesting properties such as, e.g., iridescent color, which is due to Bragg diffraction when the size of the colloid particles is comparable to the wavelength of the visible light [17,26]. Natural and artificial opals with beautiful color, which are composed of ordered silica spheres, have attracted much interest. Iridescent color in polymer dispersions has been found long ago as a consequence of the formation of liquid colloid crystals where adjacent particles repel each other because of electrostatic forces and thus order [27,28]. However, the color normally vanishes when such dispersions are dried. Due to the coalescence of polymer chains - in the case of soft polymer particles - and the loss of the water phase, the liquid colloidal crystals transform into a colorless homogeneous film, though it was shown that residual structures of the crystal ordering of the particles survive the homogenization [29]. In the case of hard polymer particles, air surrounds the ordered colloids after evaporation of the water, giving rise to a colored film; but the film is too fragile for any application [30,31]. A commonly used method to fix the crystalline colloidal arrays is via in-situ polymerization of monomers [21-25] or binders [32] around the particles making up the crystal. These routes of fabrication involve either crystallization of colloid particles in monomer-containing phase, or filling the interstitial voids of the crystal with other matrix-forming materials. Thus additional complicated pre- and post-treatment procedures are required, limiting large-scale manufacture.

In the following, an approach based on core-shell particles is described to fix the crystalline arrays such that the resultant robust large-scale polymer films exhibit beautiful angle-dependent color effects [33]. The preparation strategy is shown in Figure1: Monodisperse core-shell particles with a hard core and a soft film-forming shell were synthesized by emulsion polymerization. During drying this dispersion to thin films the polymer particles are assembling into a three-dimensional (3D) periodic structure. The soft shells deform, the polymers of adjacent shells interdiffuse, resulting in a continuous matrix. During this process the cores remain unaffected. The ordered

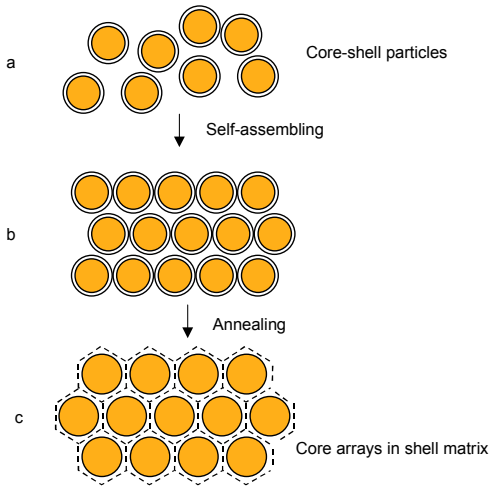

Figure 1. Schematic representation of the approach to fabricate an iridescent polymer film from core-shell particles. (a) Synthesis of the core-shell particles with a hard core and a soft shell. (b) Self-assembly into a three-dimensional crystal structure. (c) Drying and annealing to form and strengthen the film.

array of cores is responsible for the color effect. Annealing strengthens the film. By this core-shell approach, crystallization of the particles, matrix formation and annealing successively simplify the fabrication procedure.
A similar approach to fabricate 3D periodic structures of core-shell particles was reported by Kalinina and Kumacheva [34], where the core consisted of poly(methyl methacrylate) (poly(MMA)), and the shell consisted of copoly(methyl methacrylate/butyl methacrylate) (copoly(MMA/BMA)). An application for data storage was proposed. However, as far as color effects are concerned, the films did not exhibit color after drying, because the refractive index contrast between core and shell was not sufficient. Another approach pursued by Ruhl et al. employs the ordering of core-shell particles in a melt process [35,36]. In the current investigation, in order to achieve a higher refractive index contrast between core and shell, we made the cores mainly from polystyrene, which has a comparatively high refractive index (n=1.59) among polymers, and the shell from copoly(MMA/BA), which has a lower refractive index (n=1.47) and the additional ability for film formation at room temperature because of its low glass transition temperature [37,38].

Experimental section

Materials

Methyl methacrylate (MMA, 99%), n-butyl acrylate (n-BA, 99%), styrene (S, 99%), acrylic acid (AS, 99%), allyl methacrylate (AMA, 99%), a mixture of dodecyl- and tetradecyl-ethylenoxide (2.5 -EO-) sulfonic acid sodium salt (28%), sodium hydroxide solution (NaOH, 25%wt), sodium persulfate, polystyrene seed dispersion with seed size of 30 nm and solid content of 33% were used. All percentages are given as weight percents. Divinylbenzene (DVB, 98%) was purchased from Merck-Schuchardt. Deionized water is used in all experiments.

Synthesis

The reactions were performed in a 2000 ml four-necked glass reactor equipped with a reflux condenser, temperature controller, nitrogen gas inlet, monomer and initiator inlets and mechanical stirrer. Core-shell particles were synthesized using three-stage emulsion polymerization in the presence of polystyrene seed. Particles with various diameters can be obtained by changing seed and monomer amount in each stage. All reactions were carried out at 358 K and at a stirring rate of 150 rpm (with a horseshoe mixer). Prior to polymerization, the reaction mixture was purged with nitrogen and a slight positive nitrogen pressure was maintained during the reaction.
Stage 1: Synthesis of core-particles - 258.6 g water, 5.1 g polystyrene seed dispersion and 26 g sodium persulfate solution (3.6%) were pre-charged (initial feed) into the reactor and pre-reacted for 5 minutes. Then 110 g sodium persulfate solution (3.6%) and monomer-emulsion from 540.0 g S, 35.0 g n-BA, 13.3 g DVB, 10.0 g AS, 1.7g AMA, 16.4 g dodecyl- and tetradecyl-ethylenoxide (2.5 -EO-) sulfonic acid sodium salt (28%), 27.3 g NaOH solution (25%) and 501 g water were fed drop-wise over a period of 4 hours. It was assumed that the reaction ran in a starve-fed mode so as to avoid secondary nucleation. After monomer feed was completed, the reaction was continued for an additional hour, and then the system was cooled down to room temperature. The core-particle dispersion with a solid content of 40% was obtained.

Stage 2 and 3: Synthesis of core-shell particles - In the reactor, 325.8 g core-particle dispersion from the previous stage and 5 g sodium persulfate solution (1.6%) were pre-charged and pre-reacted for 5 minutes. Then 45 g sodium persulfate solution (1.6%) was fed over a period of 3 hours. During the same time, the monomer-emulsion made from 11.7 g S, 9.1 g n-BA, 1.5 g AS, 1.2 g AMA, 1.9 g dodecyl- and tetradecyl-ethylenoxide (2.5 -EO-) sulfonic acid sodium salt (28%), 1.5 g NaOH solution (25%), and 55.0 g water was fed during 45 minutes and post-reacted for 15 minutes. Then another monomer-emulsion made from 71.5 g n-BA, 34.6 g MMA, 1.3 g AS, 1.2 g dodecyl- and tetradecyl-ethylenoxide (2.5 -EO-) sulfonic acid sodium salt (28%), 0.8 g NaOH solution (25%), and 53.5 g water were fed over a period of 2 hours. Following the monomer feed, the reaction was continued for an additional hour followed by cooling down to room temperature. The core-shell particle dispersion with a solid content of 40% was obtained.

Measurement of particle size

The z-average particle diameter was obtained by photon correlation spectroscopy according to ISO 13321 in the diluted dispersions with a solid content of about 0.005%. The Autosizer IIC (Malvern Instruments, England) was used with a He-Ne laser at a wavelength of 633 nm, with a scattering angle of 90°, measured at 23°C. The value of the average particle size was obtained by the so-called cumulant analysis. The polydispersity index (P.I.=(D90 - D10)/D50) was approximately the same as the standard deviation of the particle size.

Film formation

All films were prepared by casting the dispersions on a smooth black paper or on a clean glass plate by film applicators with different gap sizes. The films were dried under ambient atmosphere. The nominal thickness of the film referred to was taken as the size of the film applicator gap except when denoted otherwise.

Characterization

The morphology of the particles and films was examined by atomic force microscopy (AFM) in the tapping mode using a nanoprobe (Digital Instrument) which is capable of recording phase images and using Si cantilevers with a force constant 35 N/m and oscillation frequencies of about 290 kHz. A Leica Ultracut UCT microtome equipped with a cryo-chamber EMFCS was used to prepare cryo-cuts of the film for AFM-microscopy. AFM imaging was performed under ambient conditions.
The sample for single core-shell particle observation was prepared in the following way: the diluted dispersion of core-shell particles was solidified by adding hexamethylol-melamine-methyl ether and p-toluene sulfonic acid which form a rigid 3-dimensional network about one day after mixing. The solidified dispersion with separated particles was cut by cryo-microtome yielding surfaces where cross-section images of single particles could be taken by AFM. It is to be noted that the sample preparation method developed in the current work is much simpler than conventional epoxy resin embedding technique. The reflection spectra of polymer films were recorded with a Hitachi U-3010 Spectrophotometer. The film was made by casting the dispersion onto the glass substrate and then drying under ambient atmosphere. The DSC thermograms were recorded with a DSC 820, serial number TA8000, from

Mettler-Toledo. Pieces of the dispersion films were packed into an aluminum pan, cooled down from room temperature to -60 °C at a rate of 20 °C/min and after 7 minutes heated up to 130 °C at a rate of 20 °C/min. The glass transition temperature was determined in the first scan as the midpoint temperature [38].

Results and discussion

AFM characterization of individual core-shell particles

Core-shell particles of different sizes with varying diameters ranging from 150 to 400nm were synthesized via adjusting seed and monomer amount in the three-stage emulsion polymerization. In Table 1 the resultant core-shell particle samples and their properties are listed. The core-shell particles with different sizes have a polydispersity index (P.I.) that is low enough for the formation of iridescent films. Each film has two glass transition temperatures confirming that there are two phases in the film, corresponding to the cores and the shells, respectively.

Figure 2 shows the cross-section AFM phase images of individual particles. In the phase images the hard polymer phase appears with a positive phase shift (bright) whereas the soft polymer phase appears with a negative phase shift (dark) [39]. It is to be seen that the polystyrene-dominated core (light spheres, from 7#) with about 200 nm in diameter (see Figure 2a) are evenly surrounded by copoly(MMA/n-BA) (dark shaded circles) with thicknesses of 30 to 40 nm (see Figure 2b, from 7#), thus demonstrating a well-defined core-shell architecture. A sharp interface between core and shell is always observed. The core and core-shell particles were slightly ellipsoidal in shape, which is assumed to be due to the shear stress exerted by the microtome. From the above results, it can be seen that well-defined core-shell particles were successfully realized by the three-stage emulsion polymerization.

Preparation of iridescent polymer films

Generally, self-assembly by sedimentation under gravitation is the most popular method to fabricate colloidal crystals from dispersions, but little control can be

Table 1 Characterization of the core-shell particles

Sample No.	Seed/ %[a)]	D_c/ nm[b)]	C:S[c)]	D_{cs}/ nm[b)]	P.I.[d)]	solid content/ wt%	Film color[e)]	T_g/°C[f)]
1#	0.33	173	1:1	215	0.11	40.2	Black-violet	0.7 / 89.6
2#	0.28	179	1:1	226	0.17	40.3	Violet	0.8 / 90.7
3#	0.22	191	1:1	241	0.22	40.2	Blue	-2.5 / 88.8
4#	0.14	221	1:1	281	0.17	40.8	Green	-4.0 / 87.8
5#	0.10	241	1:1	295	0.17	40.0	Orange	0.3 / 99.1
6#	0.09	261	1:1	321	0.23	39.9	Red	1.0 / 90.9
7#	0.18	197	1:1.5	271	0.18	40.0	Green	-4.4 / 99.0

a) Seed percentage: total amount of monomer in the whole core-shell particle. b) D_c and D_{cs}: diameters of the core and the core-shell particle, respectively. c) C:S: weight ratio of core to shell. d) P.I.: polydispersity index. e) The color of the film is recorded perpendicular to the film surface. f) T_g: glass transition temperature of the film. Because of the biphasic nature of the films two T_g values are given in each case.

exerted with respect to crystal orientation and domain size [17,20,30,31,40,41]. The time to form crystals may either be rather long, e.g., hours to weeks [40], or very short, e.g., minutes [41], depending on the chosen conditions. In the current work, we focus on short formation times for the crystals. The films were cast on a hydrophilic black paper (in order to avoid any background effect by usual white paper due to reflection of residual light passing the film) or on a clean glass plate. After the water had evaporated from the system at ambient conditions, the iridescence was observed at the surface of the dry films.

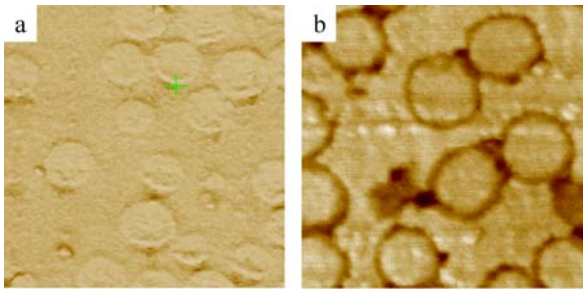

Figure 2. Cross-section AFM images of the individual particles. (a) Core-particles with a diameter (D_c) of 197 nm (7#). (b) Core-shell particles with a diameter (D_{cs}) of 271 nm (7#); the cores were taken from the sample shown in (a). The size of each picture is 1×1 μm.

The appearance of the films varied depending on the thickness of the films. In the case of thick films (250 μm) the dry film exhibited brilliant and angle-dependent color in most areas of the film (Figure 3a), but white color in the narrow edge areas (not shown in the figure). It is also noted that cracks are to be seen, as also observed in other studies [20,30,40]. The color of the film depends on the viewing angle. Looking perpendicular to the film surface, the film color varies – depending on particle size – from violet, blue, green, and orange to red, corresponding to core-shell particle diameter of 226 nm, 241 nm, 281 nm, 295 nm and 321 nm, respectively. When viewed obliquely (approximately 45°), the color changes into blue, blue-green and green, respectively. In principle, the film color can be changed continuously to cover the entire visible spectrum by adjusting the core-shell particle size.

It is seen that the core-shell particles as a film give rise to colors. After annealing at 140°C for several hours, the films had a smoother appearance while keeping their color. This result indicates that the iridescent films exhibit good thermal stability. For comparison, we also prepared a film from a core-particle dispersion. The dry film from polystyrene core-particles gave a brilliant color. However, after being exposed to elevated temperatures at 140°C only for seconds, the film became colorless, indicating the coalescence of particles. It is obvious that the coalescence of particles must be suppressed in order to get a temperature-resistant iridescent polymer film. Egen and Zentel [31] made the iridescent polymer film from highly cross linked poly(MMA/BMA) particles thus achieving that the color of the film did not vanish but changed significantly at high temperature because of the partial fusion of the particles. In the films presented here, the suppression of coalescence between core-particles was achieved by the “barrier” of the shell in the core-shell particles.

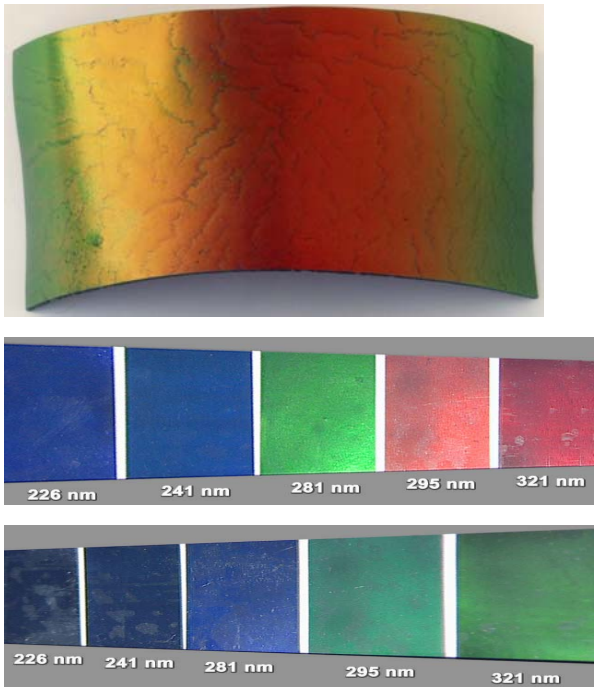

Figure 3. Iridescent polymer films with colors depending on the viewing angle and the particle size. (top) Bent film with a thickness of 250 µm. (middle) Plane film with a thickness of 60 µm. The area of each film is 4 cm × 6 cm, viewed perpendicularly. (bottom) Same as (middle) but viewed at an angle of 45°. The diameter of the core-shell particles making up the films is noted below each film.

AFM characterization

In order to illustrate how the film developed different color effects under different conditions, we investigated the microstructure of the films with different appearances by AFM.

An AFM micrograph of the brilliant area in the thick film is shown in Figure 4a. It comprises hexagonal close-packed arrays of particles with uniform orientation, suggesting that the (111) plane of fcc- or hcp-lattices is oriented parallel to the substrate[17]. The hexagonal diffraction peaks in the Fast Fourier Transform (FFT) of the image confirm the uniform orientation of hexagonal close-packed arrays on a large scale, here, of tens of micrometers. However, as is seen in Figure 4b, in the narrow edge area of the film where it is white and smooth, the crystalline order is only locally achieved - frequently being disturbed by zones with voids and disordered packing of the particles. FFT of the image reveals the lack of long range ordering (amorphous character).

The cross-sectional AFM images of the film are shown in Figure 5. In AFM images of the brilliant area in the film (Figure 5a) the ordered arrays expand from the surface to the bottom of the film, demonstrating a three-dimensional crystalline order. The pronounced diffraction peaks in FFT of the image reveal ordered packing of the particles, but the long range order is somewhat disturbed, presumably due to the process of sample preparation.

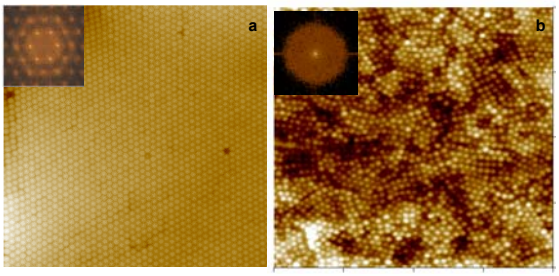

Figure 4. AFM micrographs of the surface of the thick film (with a thickness of 250 μm) from core-shell particles with particle diameter 271 nm (from 7#). The film exhibited brilliant color but was cracked. (a) Brilliant area of the film. The hexagonal close-packed arrays with uniform orientation extend over an area of tens of micrometers. (b) White area at the edge of the film. Only local ordering is seen. Fast Fourier Transform (FFT) image of each film is shown in the inset. Picture size: 10×10 μm.

It is seen in Figure 5a that the apparent size of the particles on the cross-sectional area varies periodically. This can be attributed to the deviation of the cross-sectional cut from crystal planes, as illustrated in Figure 5b, combined with mosaicity effects. If the cross-section could be prepared parallel to a crystal plane, the size of every cross-

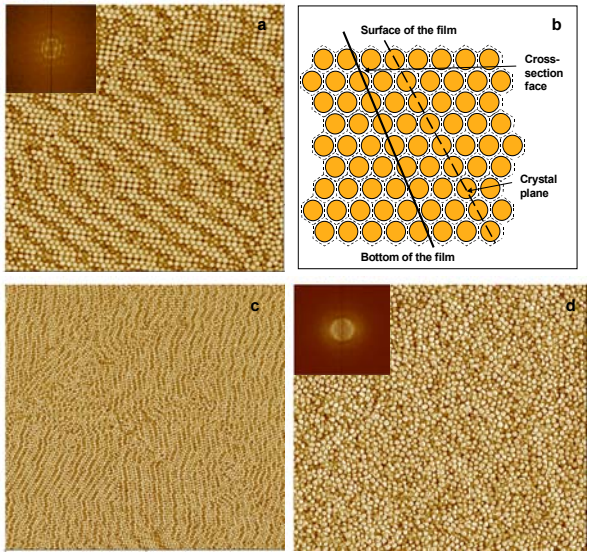

Figure 5. Cross-sectional AFM micrographs of the thick film with a thickness of 250 μm from core-shell particles with a particle diameter of 271 nm (from 7#). The film exhibits a brilliant color but is cracked; it is white and smooth in the narrow edge area of the film. (a) Brilliant area of the film. An ordered crystal structure expands over an area of tens of micrometers. (b) Illustration of a cross-sectional cut through the ordered array of particles. (c) Same film as (a), but with twofold smaller magnification. Several crystal domains with various orientations and grain boundary zones between the crystal domains are discernible. (d) White area at the edge of the film. The structure is amorphous. Fast Fourier Transform (FFT) image are shown in the inset. Picture size: (a) 10×10 μm; (c) 20×20 μm; (d) 10×10 μm.

sectioned particle would appear identical on the cross-sectional cut. Figure 5c shows a cross-section AFM image of a larger area that exhibits brilliant colors. Several crystalline domains with different orientations and grain boundary zones are seen, suggesting a polycrystalline character of the film. In the cross-section AFM images of the white area at the edge of the film, see Figure 5d, only random packing of the particles is observed, just as on the film surface of the respective piece of the film.
In summary, the AFM micrographs reveal that the brilliant films consist of three-dimensional polycrystalline arrays whereas the white parts of the film exhibit only locally organized packing of the particles. As far as color effects are concerned, the polycrystalline character does not influence the color effect strongly. As long as every single crystalline domain covers several tens of micrometers, iridescent color appears upon illumination with white light.

Reflection spectra

The shape of the reflection spectra of the thin film (60 μm) is due to the crystalline structure of the film. As seen in Figure 6, each film gives a typical reflection peak. The reflection peaks are broadened because of disorder effects. The peak positions shift to higher wavelength with the increase of particle size. There is a linear

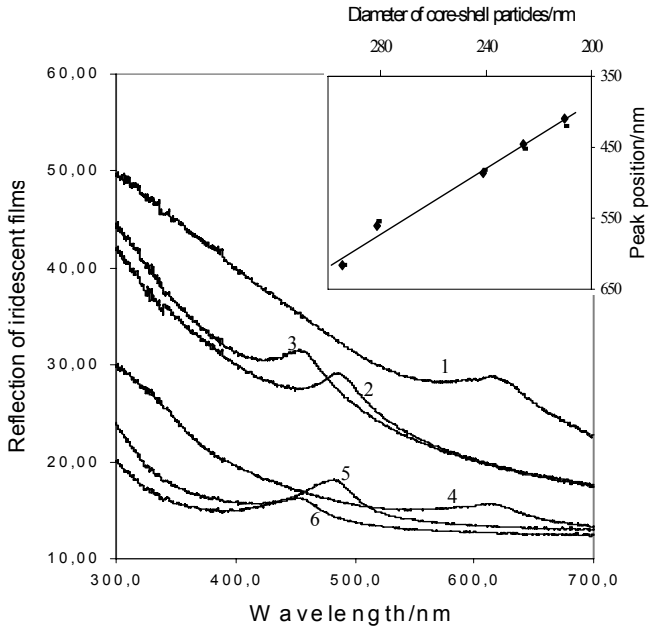

Figure 6. Reflection spectra of thin films (60 μm) made from core-shell particles with different particle diameters (the color appearance is given in brackets): 1) 295 nm (orange, 5#), 2) 241 nm (blue, 3#), 3) 226 nm (violet, 2#), 4) 295 nm (orange, 5#), 5) 241 nm (blue, 3#), 6) 226 nm (violet, 2#). Film 1, 2 and 3 were measured without annealing; film 4, 5 and 6 were measured after annealing at 140°C for one day. The wavelength of the primary reflection peak as a function of the diameter of core-shell particles is given in the inset. The straight line is a linear fit to the peak wavelength. Non-annealing (◆) and annealing (■) results are identical, indicating a temperature-resistant crystalline structure.

relationship between reflection peak position and particle size, see the inset in Figure 6, being consistent with the Bragg equation[17]. After the films were annealed at 140°C for one day, the reflection intensity of each film was reduced systematically, because the film surface became smoother thus reducing the random light scattering by the film surface, resulting in a decrease of the baseline in the reflection spectra. However, the wavelength of reflection peak remained unchanged upon annealing, indicating that the lattice constant had not changed. This is consistent with the observation that the color remains unaffected by annealing, demonstrating the good thermal stability of the iridescent films.

It was our aim to develop and describe a colored polymeric system that is storage-stable and also amenable for applications at higher temperatures. In addition, the softening of the less cross-linked shell was aimed to yield a smoother surface resulting in less light scattering, enhancing the color brilliance, as shown in Fig. 7. In Fig. 7 almost no changes in the color before and after annealing are observed. This can only

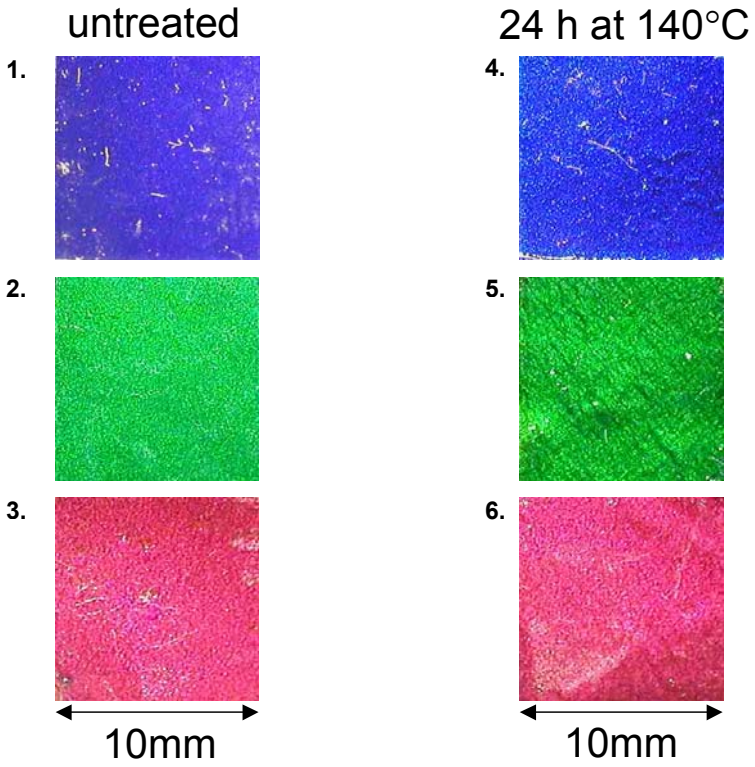

Figure 7. Color pictures of thin films (60 µm) with illumination angle of 90° and observation angle of 60° made from core-shell particles with different particle diameters (the color appearance is given in brackets): 1) 226 nm (violet, 2#), 2) 282nm (green, 4#), 3) 321 nm (red, 6#), 4) 226 nm (violet, 2#), 5) 282nm (green, 4#), 6) 321 nm (red, 6#),. Film 1, 2 and 3 were measured without annealing; film 4, 5 and 6 were measured after annealing at 140°C for one day. The wavelength of the primary reflection peak as a function of the diameter of core-shell particles is given in the inset of Fig. 6. Film colors without annealing (film 1, 2 and 3) and with annealing (film 4, 5 and 6) are almost identical, indicating a temperature-resistant crystalline structure.

be explained by assuming that no substantial changes take place in the crystalline ordering of the fused core-shell particles upon annealing. To the human eye the color brilliance appears not to be reduced but enhanced. This effect can be explained by the lower scattering level, cf. the lower baseline in Fig. 6.

Conclusions

Films made from monodisperse core-shell polymer particles according to the recipe given here exhibit brilliant iridescent color. The colored films have excellent mechanical, thermal and long-term stability. The brilliant iridescent film can be made as thin as 30 μm (in the dry state). AFM and reflection spectrum measurements demonstrate that the iridescent films had a polycrystalline structure with well-defined crystal domains. The present approach to prepare stable iridescent films allows for applications in decorative, cosmetic, and pigment industry.

References

1. López C (2203) Adv. Mater. 15:1679
2. Fudouzi H, Xia Y (2203) Langmuir 19:9653
3. Goldenberg LM, Wagner J, Stumpe J, Paulke BR, Görnitz E (2002) Mater. Sci. Eng. C22:233
4. Egen M, Voss R, Griesebock B, Zentel R, Romanov S, Sotomayor T (2003) Chem. Mater. 15 : 3786
5. Prevo BG, Velev OD (2004) Langmuir 20:2099
6. Yethiraj A, Thijssen JHJ, Wouterse A, van Blaaderen A. (2004) Adv. Mater. 16:596
7. Yethiraj A, van Blaaderen A (2003) Nature 421:513
8. Yablonovitch E (1987) Phys. Rev. Lett. 58:2059
9. Ho KM, Chan CT, Soukoulis CM (1990) Phys. Rev. Lett. 65:3152
10. Blanco A, Chomski E, Grabtchak S, Ibisate M, John S, Leonard SW, Lopez S, Meseguer F, Miguez H, Mondia JP, Ozin GA, Toader O, Van Driel HM (2000) Nature 405:437
11. Noda S (2001) MRS Bulletin 26:618
12. Joannopoulos JD, Meade RD, Winn JN (1995) Photonic Crystals. Princeton University Press. Princeton
13. Colvin VL (2001) MRS Bulletin 26:637
14. Soukoulis CM (2002) Nanotechnology 13:420
15. Stöber W, Fink A, Bohn E (1968) J. Coll. Interf. Sci. 26:62
16. Goodwin JW, Hearn J, Ho CC, Ottewill RH (1974) Coll. Polym. Sci. 252:464
17. Xia Y, Gates B, Yin Y, Lu Y (2000) Adv. Mater. 12:693
18. Norris DJ, Vlasov YA (2001) Adv. Mater. 13:371
19. Noda S, Tomoda K, Yamamoto N, Chutinan A (2000) Science 289:604
20. Wang D, Caruso F (2003) Adv. Mater. 15:205
21. Carlson RJ, Asher SA (1984) Appl. Spectrosc. 38:297
22. Asher SA (1986) U.S. Patent 4,627,689 and 4, 632, 517
23. Pan G, Kesavamoothy R, Asher SA (1997) Phys. Rev. Lett. 78: 3860
24. Lee K, Asher SA (2000) J. Am. Chem. Soc. 122: 9534
25. Foulger SH, Jiang P, Lattam A, Smith DW, Ballato J, Dausch DE, Grego S, Stoner BR (2001) Langmuir 17: 6023
26. Egen M, Braun L, Zentel R, Tannert K, Frese P, Reis O, Wulf A (2004) Macromol. Mat. Eng. 289: 158
27. Krieger IM, O'Neill FM (1968) J. Am. Chem. Soc. 90: 3114
28. Hiltner PA, Krieger IM (1969) J. Phys. Chem. 73: 2386
29. Rieger J, Hädicke E, Ley G, Lindner P.(1992) Phys. Rev. Lett. 68: 2782

30. Müller M, Zentel R, Maka T, Romanov SG, Torres CMS (2000) Chem. Mater. 12: 2508
31. Egen M, Zentel R (2002) Chem. Mater. 14: 2176
32. JP 08,231,900 [96,231,900] (1996), Eidai Co Ltd Japan, invs.: Katayama Yoshihisa, Sugita Kyoshi; Chem. Abstr. 125, 303402y
33. (a) Eilingsfeld HJ, Siemensmeyer K, Schuhmacher P, Rupaner RF, Leyrer RJ (1997) DE19717879 A1 Chem.Abstract 129 (25) 332185. (b) Rupaner R, Leyrer RJ, Schuhmacher P (1998) DE19820302 A1, Equivalent EP 955323 A1, Chem. Abstract 131 (24) 323065. (c) Hamers C, Rupaner R, Leyrer RJ, Schuhmacher P, Yang Z (1998) DE19834194 A1, Chem.Abstract 132 (11) 138857
34. Kalinina O, Kumachcheva E (1999) Macromolecules *32*: 4122
35. Ruhl T, Spahn P, Hellmann GP (2003) Polymer 44: 7625
36. Ruhl T, Spahn P, Winkler H, Hellmann GP (2004) Macromol. Chem. Phys. 205: 1385
37. Ullmann's Encyclopedia of Industrial Chemistry, the 5th Edition, p. 169
38. Penzel E, Rieger J, Schneider HA (1997) Polymer 38: 325
39. Kirsch S, Pfau A, Stubbs J, Sundberg D. (2001) Coll. Surf. A 183: 725
40. Subramania G, Constant K, Biswas R, Sigalas MM, Ho KM (2001) Adv. Mater. 13: 443
41. Dushkin CD, Lazarov GS, Kotsev SN, Yoshimura H, Nagayama K (1999) Coll. Polym. Sci. 277: 914